

Received 23 November 2022, accepted 12 December 2022, date of publication 15 December 2022, date of current version 21 December 2022.

Digital Object Identifier 10.1109/ACCESS.2022.3229677

RESEARCH ARTICLE

Realization of Three Dimensional Printed Multi Layer Wide Band Prototype

SUJAN SHRESTHA¹, (Member, IEEE), SYED MUZAHIR ABBAS^{1,2}, (Senior Member, IEEE), MOHSEN ASADNIA¹, (Senior Member, IEEE), AND KARU P. ESSELLE^{1,3}, (Fellow, IEEE)

¹School of Engineering, Faculty of Science and Engineering, Macquarie University, Sydney, NSW 2109, Australia

²BENELEC Technologies, Botany, NSW 2019, Australia

³School of Electrical and Data Engineering, University of Technology Sydney, Sydney, NSW 2007, Australia

Corresponding author: Sujan Shrestha (sujan.shrestha1@students.mq.edu.au)

This work was supported in part by the Australian Research Council (ARC), and in part by the Macquarie University International Research Excellence Scholarship (iMQRES).

ABSTRACT The three dimensional printing method is currently on stage of rapid development to realize complex nature of structure in simpler and feasible ways. In this paper, we proposed a 3D printed wideband antenna structure with high performance to improve the characteristics properties of feed source by eliminating the use of expensive superstates. A 60 mm × 60 mm × 22.5 mm wideband structure was first fabricated from VERO CMYK material through Multijet 3D printing method where the bottom layer are copper painted so as to realize the higher permittivity layer. The proposed structure is maintained at 16 mm (0.64λ) above the ground plate of 60 mm × 60 mm × 1 mm, which is feed by WR-75 waveguide. The proposed antenna is designed to have a wide operating bandwidth from 10 to 15 GHz, which cover Ku-band frequency range. Directivity enhancement is obtained over a large bandwidth by using high permittivity material for Layer 1 and lower permittivity material for Layer 2 and Layer 3. The resulting antenna prototype demonstrates a directivity bandwidth product (DBP) of 3012.79 and DBP per unit area (DBP/A) of 523.06, where directivity and gain are found to be higher than 15 dBi over the entire operating frequency band. The total area of the new antenna prototype is 2.4λ × 2.4λ × 0.9λ (4.16λ_g × 4.16λ_g × 1.56λ_g), and overall electrical height is 1.54λ at the design frequency of 12 GHz. The proposed prototype weight 36 g and overall system have weight of 118 g, which is light in weight. The measured VSWR is less than 2, which signifies wideband characteristics of overall system.

INDEX TERMS Microwave communication, radiation patterns, three dimensional (3D) printing, wide band.

I. INTRODUCTION

Wideband antennas plays a crucial role in modern and future wireless communication systems due to its high data rate, low cost and its operation in different frequencies for various wireless transmission functions. This results in several challenges in antenna design, such as antenna space limitation, design flexibility [1], [2]. The study of wideband antenna is been an exciting arena for researchers particularly with the use of dielectric slabs as observed in a prototype Electromagnetic Band gap (EBG) structure studied in [3], four layer composite superstructure applied in EBG resonator antennas (ERAs) [4], all dielectric superstrate with variation of

The associate editor coordinating the review of this manuscript and approving it for publication was Davide Ramaccia¹.

permittivity values across the design surface [5], two stacked dielectric slabs integrated with a wideband all dielectric single layer partially reflecting superstructure (PRS) with a transverse permittivity gradient (TPG) [6], compact wideband resonant cavity antennas (RCAs) with PRS made out of single dielectric material [7], RCAs with printed copper patches on its surface [8], [9]. The use of these dielectric slabs are relatively expensive and it is challenging in the design fabrication process of these structures. The phenomenon of refracted wave variation are shown by metasurfaces in [10], [11], and [12], which signifies the importance to steer radiated beam direction. Similarly, to propose the approach for wideband nature, several lens design concepts are studied [13], [14], [15]. Broadband three dimensional approximate transformation optics lens is designed with

multilayered dielectric plates by drilling holes in [16] whose height is of about 40 mm with relatively greater dimensions. Compact wideband and high gain GRIN metamaterial lens antenna system is proposed in [17] which utilizes three rectangular splited metallic strips that are etched on both side of substrate resulting in the thick layer of metamaterial. Interestingly, additive manufacturing have been growing its significance to realize the complex nature of structural design [18] and in polarization transformation from linear to circular [19]. Luneburg lens [20], Eaton lens [21], Flat Hyperbolic lens [22], 3D printed dielectric planar lens [23] are fabricated from 3D printing approach which are relatively bigger in size. Furthermore, multilayered cylindrical 3D printed dielectric lens antenna is proposed in [24], which shows relatively lower gain with in the range from 11.2 to 12.6 dB along with height of 52.5 mm. Considering these aspect of scenario, we have proposed a 3D printable wideband miniaturized prototype that could be operated in entire Ku-band, which signifies wideband properties. The Ku-band is considered as an significant band of frequencies that are utilized in modern satellite communication [25], [26]. The 3D printing approach as such Fused Deposition Modeling (FDM) have been utilize to design several prototypes [27], [28], [29], [30], [31], [32], [33], [34] and are increasing in its applicability to realize more complex type of structure. This work signifies the alternative approach to replace expensive dielectric superstrate and need for computer numerical control machining that uses variety of cutting tools as well as the use of copper spray technique to realize higher permittivity surface. The use of metal spray on 3D printed part have been studied in [35], which depicts higher gain over wide bandwidth. In this work, multilayer superstate is designed with cubes as an unit cell that are holded by three perpendicular cylindrical rods from 3D printing technology, which has many advantages compared with the traditional fabrication methods such as being easier to prototype complicated designs in terms of low cost and low weight. The proposed PRS based antenna is simple, multilayer that is suitable for manufacturing through standard bench top 3D printers. There is the dual resonator approach in PRS based antenna, however, it doesnot require any spacing to be added between each of the layers [3], [36]. The novelty of proposed approach are reduction in profile of overall antenna as well as simplified manufacturing process suitable for rapid prototyping. The proposed antenna can be applied to have light weight prototype for maintaining communication links in microwave and satellite communication network where proposed antenna could provide wide band operation thus maintaining efficient communication channel with minimum packet loss. Following sections are organized as: Design procedure for considered unit cell is explain in section "Consideration for the Design of unit cell". Similarly, the obtained phase analysis are depicted in section "Analysis of Aperture Phase distribution". The obtained radiation patterns and characteristics plots along with comparison table are discussed in section "Numerical Results

and Discussion". Finally, concluding remarks are presented in section "Conclusion".

II. CONSIDERATION FOR THE DESIGN OF UNIT CELL

The analysis to propose wideband prototype begins with the study of cubes as an unit cell. The lateral dimension of cubes varies from minimum of 0.5 mm^3 (0.02λ) to maximum of 7.5 mm^3 (0.3λ) that are holded by three perpendicular cylindrical rods of diameter 0.65 mm (0.026λ). The design frequency is 12 GHz ($\lambda = 25 \text{ mm}$), which is middle frequency of operating WR-75 waveguide. The frequency is chosen in order to have higher directivity over wide bandwidth in small footprint. The ground plane and PRS have equal lateral dimensions of $2\lambda \times 2\lambda$ (where, λ is wavelength at design frequency). Two ports 1 and 2 are kept at $h = 12.5 \text{ mm}$ ($\lambda/2$) distance far from top and bottom surface of cylindrical rod as shown in Figure 1(a). We have studied the transmission coefficient parameters of cubes with two different dielectric constant values of 3 and 10. The transmission coefficient is represented by, τ , whereas reflection coefficient is denoted by, ∂ . The reflection coefficient of analysed unit cell is below -10 dB . These cubes are placed in Reference Plane 1 at level of $h_1 = 12.5 \text{ mm}$ ($\lambda/2$), in defined aperture position as per the need of required phase $\phi_{RP1}(x,y)$ so as to obtain the uniform phase variation $\phi_{RP2}(x,y)$ in Reference Plane 2. The Reference Plane 2 lies closer to top surface of proposed wideband prototype, which is at 3.125 mm ($\lambda/8$) and overall $h_2 = 25.63 \text{ mm}$ (1.03λ). The diagram for relative placement of layers in defined positions are shown in Figure 1(b), where Layer 1 cubes are obtained from dielectric constant value of 10 where as Layer 2 and Layer 3 cubes are analyzed from dielectric constant value of 3. The PRS is placed at a height, $h_1 = 12.5 \text{ mm}$ ($\lambda/2$), above the ground plane, which is made out of aluminum. To feed the cavity-formed between ground plane and PRS, a rectangular slot with dimension $19.1 \text{ mm} \times 9.5 \text{ mm}$, is cut out in middle of ground plane. This slot, which acts as primary excitation source for proposed antenna, is then interfaced with a standard WR-75 waveguide-to-coax transition. The PRS of the antenna is required to provide necessary transmission magnitude ($|S_{21}| > 0.8$) to provide the necessary gain enhancement by creating an effective resonant cavity between itself and ground plane. The gain bandwidth of antenna and quality of radiation patterns can, however, be further improved, by utilizing more than one reflective layer or so-called multiple-resonators within PRS [3]. For this purpose, proposed PRS shown in Figure 1(b) is composed of three layers. Each of the layers is made out of 8×8 unit-cells, whereas each unit-cell is a cube.

In design frequency, variation of cube sizes results in change of magnitude and phase values of transmission coefficient as shown in Figure 2. The material Dk3, with dielectric constant 3 have greater transmission magnitude above 0.95 but phase range is obtainable from 0° to 80° .

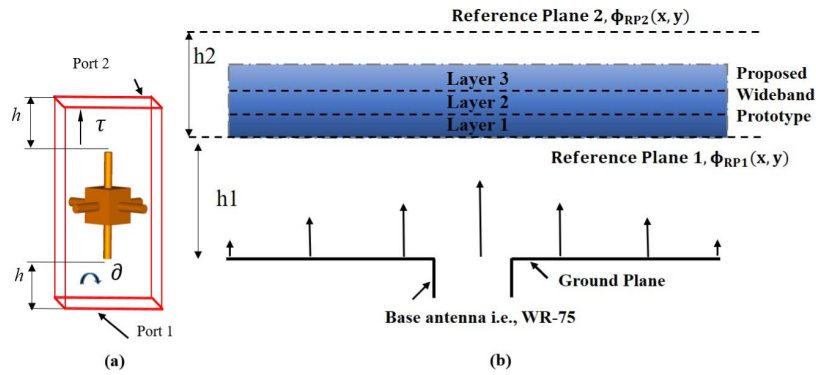


FIGURE 1. (a) Unit Cell under consideration (b) System diagram for the placement of proposed wideband prototype.

Interestingly, material Dk10, with dielectric constant 10 shows transmission magnitude of about 0.95 that remain constant for cube size of 5.5 mm^3 afterward it drops significantly from 0.97 to 0.68 and then increases to about 0.92 for maximum cube size. Similar pattern in observed in case of phase variation where it varies from 80° to 0° till the cube size reach to 5.5 mm^3 and marked increase in phase to 330° is seen which gradually drop to 225° . This variation is due to cube being more reflective as its size reaches to 5.5 mm^3 . The full stack of three-unit cells will not be suitable to analyze because of different materials under consideration for each layer. Individual layer of cube is analyzed to generate uniform phase distribution starting from higher permittivity in bottom layer to lower permittivity in successive two layers. The independently simulated cube's result for transmission coefficient magnitude and phase is shown in Figure 2 with respective material under consideration, which signifies the response of each stack. The normalized phase distribution is used to maintain the respective cubes in defined aperture positions.

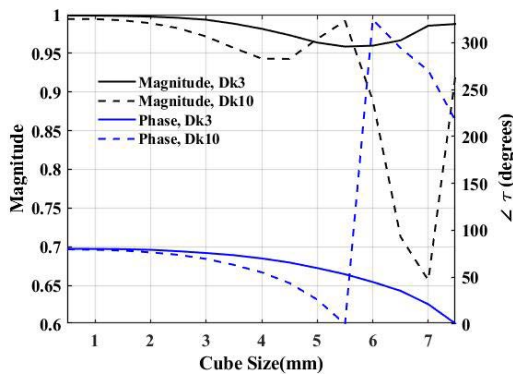


FIGURE 2. Simulated Distribution of Transmission Coefficient Magnitude and Phase plots for two different materials.

III. ANALYSIS OF APERTURE PHASE DISTRIBUTION

Initially, we have started with noting phase above WR-75 waveguide only, which shows greater phase variation

of about 210° . This phase is corrected to about 49° after placement of cubes in Layer1 which are obtained from Dk10 at 12.5 mm ($\lambda/2$) distance away from feed source. Furthermore, phase is corrected to 37° by placing cubes obtained from Dk3 in Layer 2. Finally, cubes of Dk3 are kept in Layer 3 to have fine adjustment in phase variation. The overall variation of phase distribution are shown in Figure 3.

A. PLACEMENT OF RELATIVE CUBES ACROSS THE APERTURE

Unlike in previous multi-layer PRSs, there are no effective gaps between layers, thus reducing overall profile. Note that blocks in any one layer have a fixed size, and this size of unit-cell blocks determines overall reflectivity provided by that layer. The reflective properties of unit-cells were studied using superstrate reflection model [37]. The pictorial diagram for the top, side and perspective views of proposed structure is shown in Figure 4.

In order to realize proposed wideband prototype, we have considered three different layers and individual layers are composed of four different rounds where designed cube sizes are arranged in rectangular patterns due to its significance

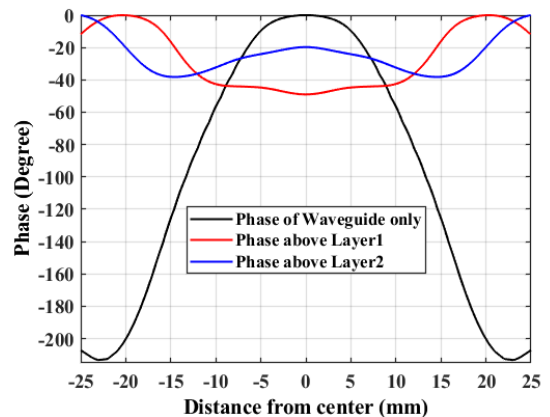


FIGURE 3. Simulated overall phase distribution across the aperture of proposed system.

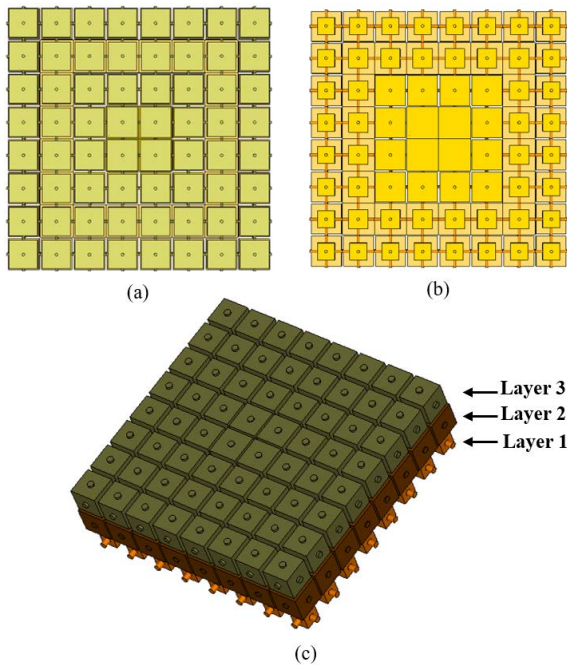


FIGURE 4. Overall view of proposed designed prototype (a) Top view (b) Bottom view (c) Perspective view.

to improve characteristics properties of feed source [38]. The pictorial description for arrangement of several rounds of unit-cells in each layer are described in [29]. We have used four different stacks of unit-cells in each layer. The unit cell of single cube is considered to generate respective layers for overall three layers of proposed prototype. To signify the effect of these unit cell over band of interest, we have plotted phase distribution from 10 to 15 GHz frequency band. The Rounds signify arrangement of cubes across defined aperture positions in each layer starting from central position which is Round 1 and successively moving towards the end portion which is Round 4. In Layer 1, four different rounds as Round 1, Round 2, Round 3 and Round 4 have cube sizes of 7.5 mm^3 , 7 mm^3 , 4.5 mm^3 and 4 mm^3 . Additionally, in Layer 2, Round 1, Round 2, Round 3 and Round 4 have cube sizes of 6 mm^3 , 6.5 mm^3 , 7.5 mm^3 and 7 mm^3 . Similarly, in Layer 3, Round 1, Round 2, Round 3 and Round 4 have cube sizes of 7 mm^3 , 6.5 mm^3 , 6.5 mm^3 and 6.5 mm^3 . The size is linear dimension of cubes across its length, breadth and height. Note, that the variation of cube sizes within each layer can provide further degree of freedom in PRS. Since, the proposed PRS is required to be suitable for manufacturing through standard bench-top 3D printers, material selected for Layer2 and Layer3 is Premix Preperm ABS300 (permittivity (ϵ_r) = 3, loss tangent ($\tan\delta$) = 0.004) and that for Layer1 is Premix Preperm ABS1000 (permittivity (ϵ_r) = 10, loss tangent ($\tan\delta$) = 0.003). The reflectivity ($|S_{11}|$) computed for each of these layers in 12 GHz, using CST-MWS time-domain solver are -13.2 dB , -14.5 dB and -17.2 dB for Layer1, Layer2 and Layer3 respectively in design frequency. The overall system diagram is shown in Figure 5, which

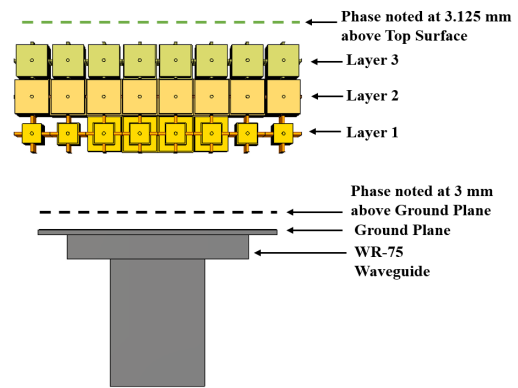


FIGURE 5. Overall system setup and placement of proposed wideband prototype above the feed source.

shows relative positions to note phase distributions along with placement of proposed wideband prototype.

B. VARIATION OF PHASE DISTRIBUTION OVER DIFFERENT FREQUENCIES

The phase distribution are noted near feed source in 3 mm (0.12λ) distance above ground plane, which is the condition of phase without placement of wideband prototype. Similarly, phase is noted in 3.125 mm (0.125λ) just above top surface of wideband prototype after its placement in 12.5 mm ($\lambda/2$) above ground plane. The phase distribution shown in Figure 6 and Figure 7 signifies uniform distribution across defined aperture dimension. The phase variation is less than 50° over most of frequency of interest. The more sample of phase distribution is added to signifies variation observed in phase before and after the placement of proposed prototype above feed WR-75 waveguide. The noted phase variation without and with placement of proposed prototype above ground plane for 10 GHz, 11 GHz, 12 GHz are shown in Figure 6 (a), (c), (e) and Figure 6 (b), (d), (f) respectively. Similarly, phase pattern noticed for 13 GHz, 14 GHz, 15 GHz without and with placement of proposed prototype above ground plane are shown in Figure 7 (a), (c), (e) and Figure 7 (b), (d), (f) respectively. The phase variation obtained after calculation of difference in phase value from centre and of end aperture position for 10 GHz, 11 GHz, 12 GHz, 13 GHz, 14 GHz and 15 GHz are respectively 211.74° , 240.65° , 270.45° , 299.97° , 329.53° , 362.29° which was calculated without the placement of proposed structure. These values are further corrected, and more uniform phase distribution are observed after placement of proposed structure. Thus, respective corrected phase values are 62.84° , 162.76° , 69.11° , 187.96° , 176.45° , 133.02° for 10 GHz, 11 GHz, 12 GHz, 13 GHz, 14 GHz and 15 GHz frequencies. The phase maps are not symmetric due to the effect of proposed prototype and uniformity in phase variation is more prominent for 12 GHz as it is the operating frequency and over the wide band of frequencies more variation in phase distribution is noticed.

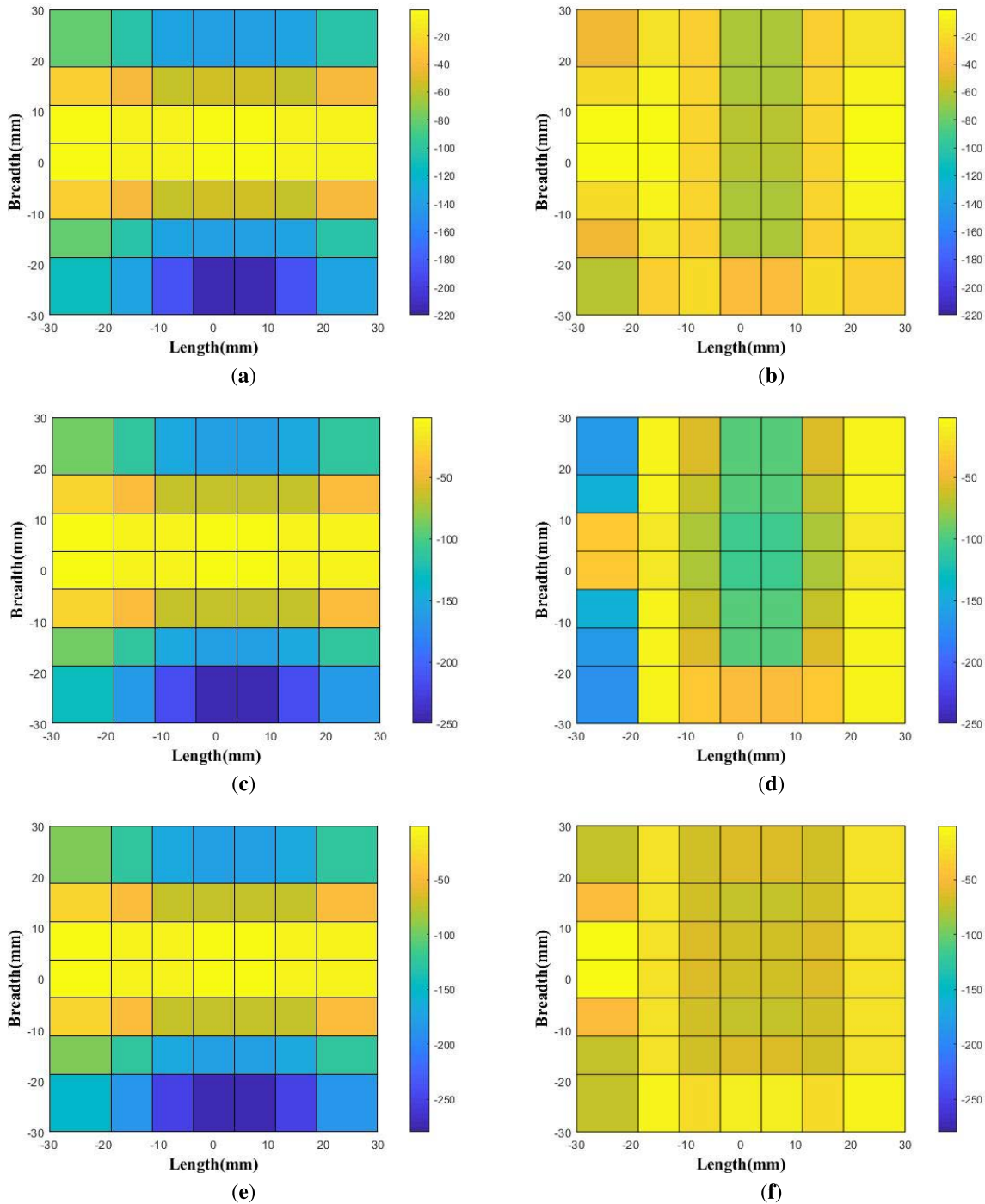


FIGURE 6. Aperture Phase distribution noted above the feed WR-75 waveguide without the proposed prototype (a) at 10 GHz, (c) at 11 GHz, and (e) at 12 GHz and with the placement of the proposed prototype (b) at 10 GHz, (d) at 11 GHz, and (f) at 12 GHz.

The uniformity in E-field phase distribution is observed after the placement of proposed prototype above the feed WR-75 waveguide as shown in Figure 8 (a), (b). This figure shows additional phase profile impressed by placement of proposed prototype which signifies the uniformity in phase distribution. The field distribution is generated to be uniform for each layer as noted from Figure 8 (b).

IV. NUMERICAL RESULTS AND DISCUSSION

This section describes fabrication and measurement results of proposed wideband prototype along with its characteristics plots.

A. DETAIL OF FABRICATION AND MEASUREMENT SETUP

The Multijet 3D printing technique is used to fabricate proposed structure as it utilizes resin which mimic properties of

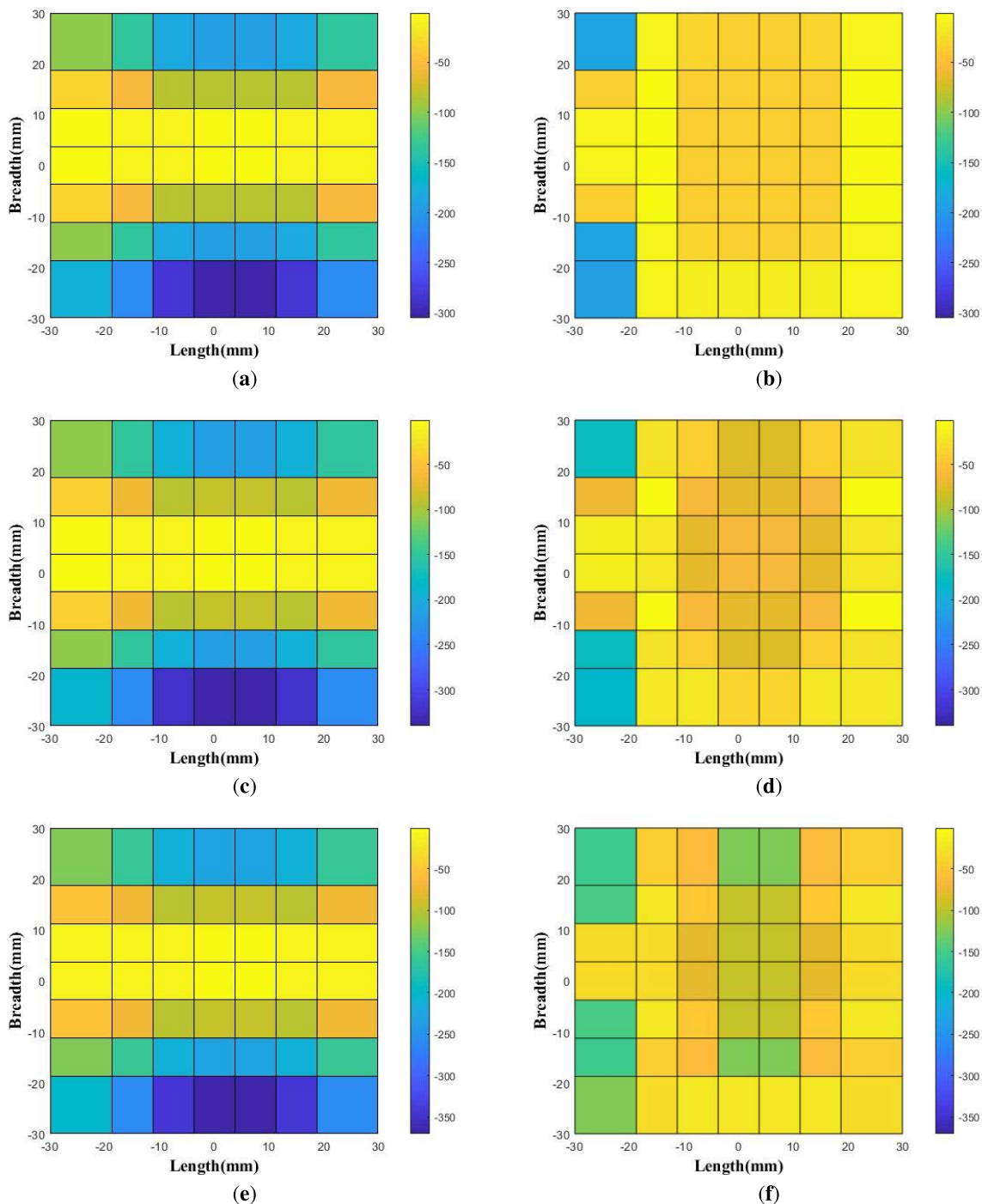


FIGURE 7. Aperture Phase distribution noted above the feed WR-75 waveguide without the proposed prototype (a) at 13 GHz, (c) at 14 GHz, and (e) at 15 GHz and with the placement of the proposed prototype (b) at 13 GHz, (d) at 14 GHz, and (f) at 15 GHz.

Premix Preperm ABS300. Multijet 3D printing have ability to print small dimension object with resolution of about 0.01 mm. In contrast, Fused Deposition Modeling (FDM) is not been able to print small size cubes along with supporting cylindrical rods. Eventhough whole structure is fabricated from resin, we have copper painted the lower Layer 1 considering that this layer shall shows characteristics performance similar to Premix Preperm ABS1000. The use of

copper solution to Acrylonitrile Butadiene Styrene (ABS) fabricated prototype is studied in [30], which was compared with structure fabricated from Premix Preperm ABS1000 filament. The measurement setup is performed in NSI-700S-50 spherical near field measurement system at Australian Antenna Measurement Facility, which is shown in Figure 9. The attached figures show top surface of fabricated prototype, copper painted bottom surface and overall assembled

TABLE 1. Comparison of proposed wideband prototype against the available 3D printed antenna structures.

Ref.	Electrical Height from Feed (mm)	Footprint (mm*mm*mm)	Peak Directivity (dBi)	Peak Gain (dBi)	Bandwidth (%)	3dB Bandwidth (%)	Side Lobe Level E-plane (dB)	Side Lobe Level H-plane (dB)	Directivity Bandwidth Product (DBP) (%)	Polarization	Fabrication Method	Weight (g)
Proposed	1.54λ (38.5)	2.4λ×2.4λ×0.9λ (60×60×22.5)	17.8	17.5	50	20	-20	-15	1205.12	Linear	Multijet 3D printing	118 g
[19]	0.194λ (0.97)	3.8λ×3.8λ×2.58λ (19×19×12.89)	16	15	50	30	-15	n/a	1194.32	Circular	Polyjet 3D printing	n/a
[30]	1.17λ (29.33)	2λ×2λ×0.49λ (50×50×12.33)	17.6	17.2	50	20	-14.2	-16.9	1150.87	Linear	Fused Deposition Modeling (FDM)	79 g with copper painted; 96 g with PREPERM10
[32]	1.39λ (41.8)	4λ×4λ×0.78λ (120×120×23.3)	17.8	16.1	30	15.79	-9	-12	951.44	Linear	Fused Deposition Modeling (FDM)	n/a
[33]	0.99λ (27.2)	1.97λ×1.97λ×0.49λ (54×54×13.5)	16.05	n/a	49.65	20.32	n/a	-12.7	1999	Linear	Fused Deposition Modeling (FDM)	15.6
[34]	0.83λ (20)	4.9λ×4.9λ×0.37λ (140×140×50.76)	n/a	13.5	59	n/a	n/a	n/a	n/a	Linear	Fused Deposition Modeling (FDM)	n/a

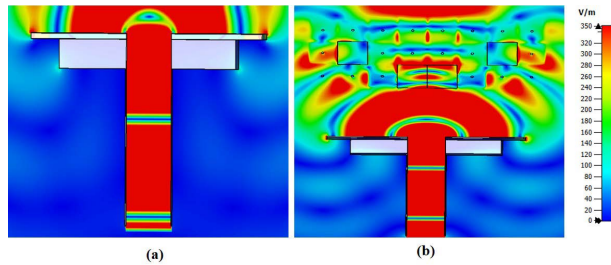


FIGURE 8. Distribution of E-field (a) Waveguide only (b) After the placement of proposed prototype above feed WR-75 Waveguide.

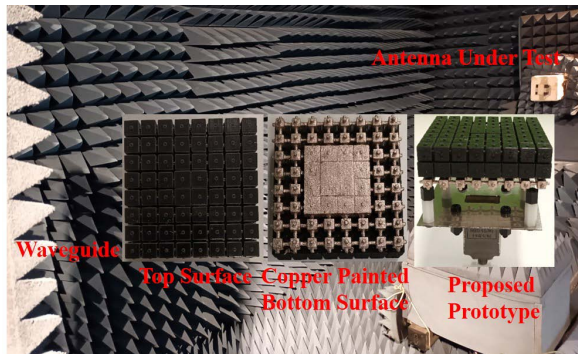


FIGURE 9. Measurement system showing the experimental setup of proposed wideband prototype.

system, where proposed prototype is kept above feed WR-75 waveguide. Hence, it is compared against simulated results as obtained from commercial software CST Microwave studio. These are detailed in further sections, including radiation plots and characteristics features.

B. DISTRIBUTION OF RADIATION PATTERNS OVER WIDEBAND FREQUENCIES

The E-plane and H-plane radiation patterns of proposed system are shown in Figure 10a-f for 10 GHz, 11 GHz, 12 GHz, 13 GHz, 14 GHz, and 15 GHz frequencies respectively, which shows narrow-beamwidth, broadside directed beam over 3dB bandwidth. The 3dB angular width and Side Lobe Level (SLL) in E- and H- planes are significantly improved after

placement of proposed prototype above feed source. Considering feed WR-75 waveguide source only, in E-plane 3dB angular width and side lobe level are 121.1⁰, 54.7⁰, 114⁰, 128.8⁰, 128.8⁰, 118.7⁰; -14.1, -14.3, -13.8, -14.1, -15.5, -17.1 dB respectively where as in H-plane 3dB angular width and Side Lobe Level are 73.6⁰, 73.3⁰, 68.7⁰, 55.9⁰, 52.1⁰, 52⁰; -14.6, -13.4, -13.7, -14.8, -16.1, -18.6 dB. The radiated beam patterns becomes more smooth with less 3dB angular width and lower side lobe level. After placement of proposed wideband prototype above feed source, observed 3dB angular width and side lobe level in E-plane are 24.5⁰, 20.2⁰, 17.1⁰, 16.3⁰, 15.9⁰, 13.9⁰; -15, -12.1, -14, -10.3, -11.3, -9.6 dB respectively where as in H-plane 3dB angular width and Side Lobe Level are 28.1⁰, 23.2⁰, 20.7⁰, 21⁰, 22.2⁰, 19.1⁰; -16.6, -16.9, -17.4, -13.7, -19, -18.5 dB. The worst-case side-lobe levels noted in E- and H- planes, respectively are -20 dB and -15 dB. In design frequency of 12 GHz, observed cross polarization values are below -7 dBi. However, most of values lies in between -15 dBi to -35 dBi, which signifies better matching behavior in operating frequency range.

C. CHARACTERISTIC PLOTS AND COMPARISON TABLE

Addition of successive layers improve characteristic of WR-75 source as they are kept in λ/2 distance from it as depicted in Figure 11. In operating frequency band average directivity is around 7.5 dBi. This is improved to more than 12 dBi as Layer1 is kept above WR-75. Additionally, based in phase distribution above Layer1, addition of Layer2 further improves directivity by around 2 dBi through out the operating frequency band. Finally, addition of Layer3 resulted further improvement in directivity with around 1 dBi over operating frequency band that resulted in directivity and gain of above 15 dBi over entire frequency of interest. The simulated gain and directivity are well matched against measured results, which signifies efficient operation of proposed antenna prototype. The results obtained through these studies predicted that proposed antenna has a VSWR 2:1 bandwidth from 10 GHz to 15 GHz (50% of 3dB directivity Bandwidth) as shown in Figure 12, where the simulated and measured results are conformed to each other. The VSWR are generally

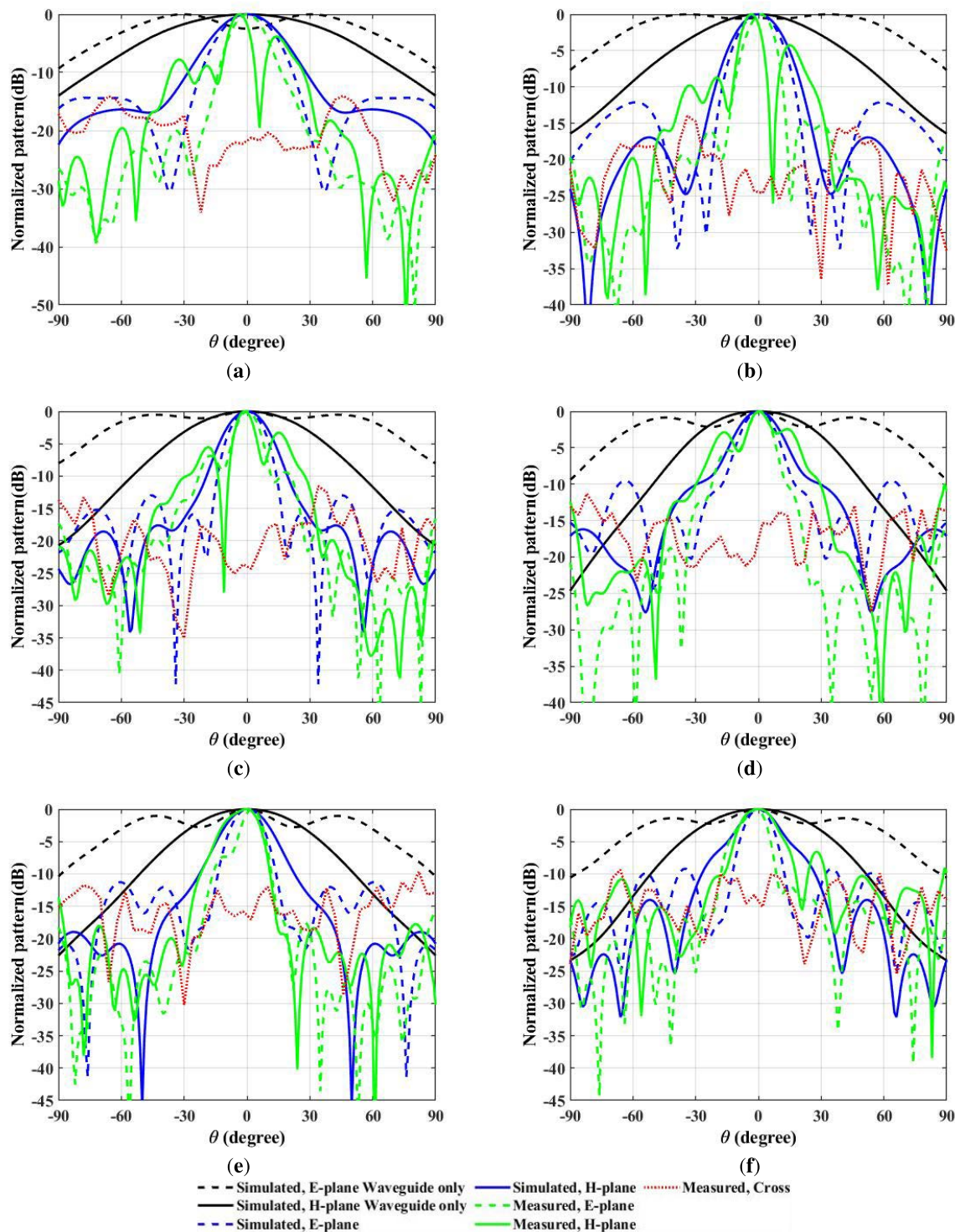


FIGURE 10. Simulated and measured radiation patterns as observed with the use of the proposed designed surface above the feed source are shown in Figure 10 (a-f) for 10 GHz, 11, GHz, 12 GHz, 13 GHz, 14 GHz, and 15 GHz frequencies.

higher from 2.5 to 2.8 around 17 to 18 GHz because of frequency limitation of WR-75 waveguide. The performance of WR-75 with and without proposed prototype is well matched with simulated results in frequency band from 10 to 15 GHz, so we have considered this frequency band for phase and

characteristics performance analysis. Similarly, comparison of proposed antenna prototype with other structure is shown in Table 1. This shows proposed 3D printed antenna prototype generate smaller footprint area with higher peak directivity and gain values across 10 to 15 GHz of operating frequency

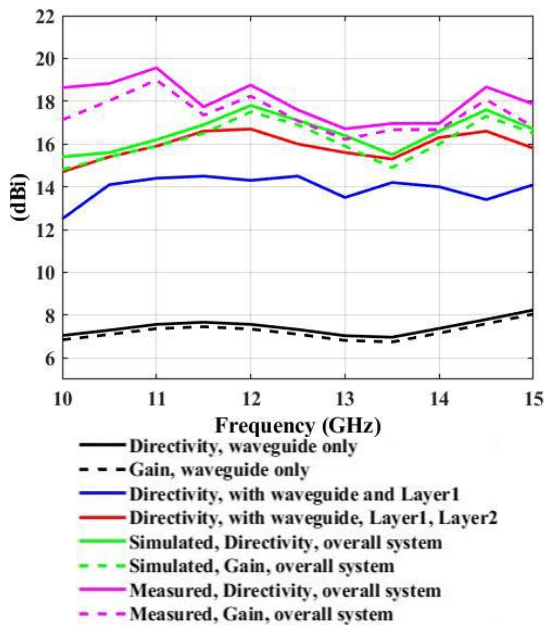


FIGURE 11. Distribution of simulated and measured directivity and gain values.

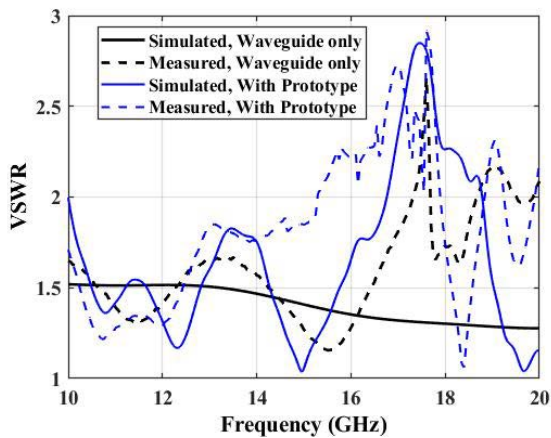


FIGURE 12. Simulated and measured VSWR plots.

bands. Additionally, this prototype shows higher 3dB bandwidth with lower side lobe levels across E- and H-planes, which is light in weight.

V. CONCLUSION

We have presented an approach to improve broadside gain of a simple ground-plane backed slot antenna, by showing a multi-layer PRS that is suitable for manufacturing with standard, bench-top 3D printers, which utilizes Multijet 3D printing method. The effectiveness of proposed approach is validated by numerically studying performance of a PRS-based antenna in CST-MWS. The resulting antenna is wideband in nature operating from 10 to 15 GHz (50% of 3dB directivity Bandwidth) predicts a best-case improvement of 15 dBi in broadside directivity. In E-plane sidelobe level are less than -20 dB through out the operating frequency band in

contrast to H-plane where it is below -15 dB. The weight of overall proposed system is about 118 g, which shows system is light in weight. Similarly, simulated and measured VSWR plots are less than 2 over frequency of interest. This signifies matching over operating frequency range that cover Ku-band region.

CONFLICTS OF INTEREST

The authors declare no conflict of interest.

ACKNOWLEDGMENT

The authors would like to thank CSIRO, Marsfield, NSW, Australia, and Macquarie University for providing support for measurement of antenna prototype.

REFERENCES

- [1] S. A. Schelkunoff, *Advanced Antenna Theory*. Hoboken, NJ, USA: Wiley, 1952.
- [2] C. A. Balanis, *Antenna Theory: Analysis and Design*. Hoboken, NJ, USA: Wiley, 2015.
- [3] R. M. Hashmi, B. A. Zeb, and K. P. Esselle, "Wideband high-gain EBG resonator antennas with small footprints and all-dielectric superstructures," *IEEE Trans. Antennas Propag.*, vol. 62, no. 6, pp. 2970–2977, Jun. 2014.
- [4] R. M. Hashmi and K. P. Esselle, "A wideband EBG resonator antenna with an extremely small footprint area," *Microw. Opt. Technol. Lett.*, vol. 57, no. 7, pp. 1531–1535, 2015.
- [5] R. M. Hashmi and K. P. Esselle, "A class of extremely wideband resonant cavity antennas with large directivity-bandwidth products," *IEEE Trans. Antennas Propag.*, vol. 64, no. 2, pp. 830–835, Feb. 2016.
- [6] A. Baba, R. Hashmi, M. Asadnia, L. Matekovits, and K. Esselle, "A stripline-based planar wideband feed for high-gain antennas with partially reflecting superstructure," *Micromachines*, vol. 10, no. 5, p. 308, May 2019.
- [7] A. A. Baba, R. M. Hashmi, K. P. Esselle, and A. R. Weily, "Compact high-gain antenna with simple all-dielectric partially reflecting surface," *IEEE Trans. Antennas Propag.*, vol. 66, no. 8, pp. 4343–4348, Aug. 2018.
- [8] F. Meng and S. K. Sharma, "A wideband resonant cavity antenna with compact partially reflective surface," *IEEE Trans. Antennas Propag.*, vol. 68, no. 2, pp. 1155–1160, Feb. 2020.
- [9] A. Lalbakhsh, M. U. Afzal, K. P. Esselle, S. L. Smith, and B. A. Zeb, "Single-dielectric wideband partially reflecting surface with variable reflection components for realization of a compact high-gain resonant cavity antenna," *IEEE Trans. Antennas Propag.*, vol. 67, no. 3, pp. 1916–1921, Mar. 2019.
- [10] J. P. S. Wong, A. Epstein, and G. V. Eleftheriades, "Reflectionless wide-angle refracting metasurfaces," *IEEE Antenn. Wireless Propag. Lett.*, vol. 15, pp. 1293–1296, 2016.
- [11] V. G. Ataloglou and G. V. Eleftheriades, "Arbitrary wave transformations with Huygens' metasurfaces through surface-wave optimization," *IEEE Antennas Wireless Propag. Lett.*, vol. 20, no. 9, pp. 1750–1754, Sep. 2021.
- [12] L. Stefanini, A. Rech, D. Ramaccia, S. Tomasin, A. Toscano, F. Moretto, and F. Bilotti, "Multibeam scanning antenna system based on beamforming metasurface for fast 5G NR initial access," *IEEE Access*, vol. 10, pp. 65982–65995, 2022.
- [13] A. Kalvach and Z. Szabó, "Aberration-free flat lens design for a wide range of incident angles," *J. Opt. Soc. Amer. B, Opt. Phys.*, vol. 33, no. 2, pp. A66–A71, 2016.
- [14] P. Castillo-Tapia, O. Zetterstrom, A. Algaba-Brazalez, L. Manholm, M. Johansson, N. J. G. Fonseca, and O. Quevedo-Teruel, "Two-dimensional beam steering using a stacked modulated geodesic Luneburg lens array antenna for 5G and beyond," *IEEE Trans. Antennas Propag.*, early access, Oct. 31, 2022, doi: 10.1109/TAP.2022.3217175.
- [15] O. Zetterstrom, N. J. G. Fonseca, and O. Quevedo-Teruel, "Compact half-Luneburg lens antenna based on a glide-symmetric dielectric structure," *IEEE Antennas Wireless Propag. Lett.*, vol. 21, no. 11, pp. 2283–2287, Nov. 2022.
- [16] H. F. Ma and T. J. Cui, "Three-dimensional broadband and broad-angle transformation-optics lens," *Nature Commun.*, vol. 1, no. 1, pp. 1–7, Dec. 2010.

- [17] B. P. Mishra, S. Sahu, S. K. S. Parashar, and S. K. Pathak, "A compact wideband and high gain GRIN metamaterial lens antenna system suitable for C, X, Ku band application," *Optik*, vol. 165, pp. 266–274, Jul. 2018.
- [18] D. Helena, A. Ramos, T. Varum, and J. N. Matos, "Antenna design using modern additive manufacturing technology: A review," *IEEE Access*, vol. 8, pp. 177064–177083, 2020.
- [19] K. X. Wang and H. Wong, "A wideband millimeter-wave circularly polarized antenna with 3-D printed polarizer," *IEEE Trans. Antennas Propag.*, vol. 65, no. 3, pp. 1038–1046, Mar. 2017.
- [20] M. Liang, W. R. Ng, K. Chang, K. Gbele, M. E. Gehm, and H. Xin, "A 3-D Luneburg lens antenna fabricated by polymer jetting rapid prototyping," *IEEE Trans. Antennas Propag.*, vol. 62, no. 4, pp. 1799–1807, Apr. 2014.
- [21] G. Du, M. Liang, R. A. Sabory-Garcia, C. Liu, and H. Xin, "3-D printing implementation of an X-band Eaton lens for beam deflection," *IEEE Antennas Wireless Propag. Lett.*, vol. 15, pp. 1487–1490, 2016.
- [22] J. M. Poyanco, F. Pizarro, and E. Rajo-Iglesias, "Wideband hyperbolic flat lens in the Ka-band based on 3D-printing and transformation optics," *Appl. Phys. Lett.*, vol. 118, no. 12, Mar. 2021, Art. no. 123503.
- [23] J.-M. Poyanco, F. Pizarro, and E. Rajo-Iglesias, "Cost-effective wideband dielectric planar lens antenna for millimeter wave applications," *Sci. Rep.*, vol. 12, no. 1, pp. 1–10, Mar. 2022.
- [24] P. Mahouti, M. A. Belen, F. Güneş, and R. Yurt, "Design and realization of multilayered cylindrical dielectric lens antenna using 3D printing technology," *Microw. Opt. Technol. Lett.*, vol. 61, no. 5, pp. 1400–1403, May 2019.
- [25] S. Shrestha and D.-Y. Choi, "Characterization of rain specific attenuation and frequency scaling method for satellite communication in South Korea," *Int. J. Antennas Propag.*, vol. 2017, pp. 1–16, Jan. 2017.
- [26] S. Shrestha and D.-Y. Choi, "Rain attenuation study at Ku-band over earth-space path in South Korea," *Adv. Astron.*, vol. 2019, pp. 1–12, Mar. 2019.
- [27] S. Shrestha, H. Zahra, M. A. B. Abbasi, M. Asadnia, and S. M. Abbas, "Increasing the directivity of resonant cavity antennas with nearfield transformation meta-structure realized with stereolithography," *Electronics*, vol. 10, no. 3, p. 333, Feb. 2021.
- [28] S. Shrestha, A. A. Baba, S. M. Abbas, M. Asadnia, and R. M. Hashmi, "A horn antenna covered with a 3D-printed metasurface for gain enhancement," *Electronics*, vol. 10, no. 2, p. 119, Jan. 2021.
- [29] S. Shrestha, H. Zahra, S. M. Abbas, A. Kiyani, B. Mohamadzade, and M. Asadnia, "Generation of beam tilt through three-dimensional printed surface," *Electronics*, vol. 10, no. 24, p. 3174, Dec. 2021.
- [30] S. Shrestha, H. Zahra, A. Kiyani, M. Asadnia, S. M. Abbas, and A. Mahmood, "Miniaturized wideband antenna prototype operating over the Ku-band," *Micromachines*, vol. 13, no. 3, p. 471, Mar. 2022.
- [31] S. Shrestha, S. M. Abbas, M. Asadnia, and K. P. Esselle, "Steering of beam using cylindrical arrangements in a metallic parallel plates structure operating over Ku-band," *Appl. Sci.*, vol. 12, no. 12, p. 6074, Jun. 2022.
- [32] C. Ponti, P. Baccarelli, S. Ceccuzzi, and G. Schettini, "Tapered all-dielectric EBGs with 3-D additive manufacturing for high-gain resonant-cavity antennas," *IEEE Trans. Antennas Propag.*, vol. 69, no. 5, pp. 2473–2480, May 2021.
- [33] T. Hayat, M. U. Afzal, F. Ahmed, S. Zhang, K. P. Esselle, and Y. Vardaxoglou, "Low-cost ultrawideband high-gain compact resonant cavity antenna," *IEEE Antennas Wireless Propag. Lett.*, vol. 19, no. 7, pp. 1271–1275, Jul. 2020.
- [34] Y. Asci and K. Yegin, "Three-dimensional printed wideband, dual-cavity Ku-band antenna," *Int. J. RF Microw. Comput.-Aided Eng.*, vol. 30, no. 4, Apr. 2020, Art. no. e22071.
- [35] S. Alkaraki, Y. Gao, S. Stremsoerfer, E. Gayets, and C. G. Parini, "3D printed corrugated plate antennas with high aperture efficiency and high gain at X-band and Ka-band," *IEEE Access*, vol. 8, pp. 30643–30654, 2020.
- [36] A. R. Weily, K. P. Esselle, T. S. Bird, and B. C. Sanders, "Dual resonator 1-D EBG antenna with slot array feed for improved radiation bandwidth," *IET Microw. Antennas Propag.*, vol. 1, no. 1, pp. 198–203, Feb. 2007.
- [37] B. A. Zeb, R. M. Hashmi, K. P. Esselle, and Y. Ge, "The use of reflection and transmission models to design wideband and dual-band Fabry–Pérot cavity antennas," in *Proc. Int. Symp. Electromagn. Theory*, May 2013, pp. 1084–1087.
- [38] S. Shrestha, B. Mohamadzade, A. A. Baba, and R. M. Hashmi, "Effect of unit cell arrangements in near field transformation lattice on aperture efficiency of resonant cavity antenna," in *Proc. Int. Conf. Electromagn. Adv. Appl. (ICEAA)*, Sep. 2019, pp. 370–371.



SUJAN SHRESTHA (Member, IEEE) received the bachelor's degree in electronic and communication engineering from Tribhuvan University, Nepal, in 2010, and the master's degree in information and communication engineering from Chosun University, Gwangju, South Korea, in 2017. He has worked as an Engineer at companies, such as Huawei and broadcasting firms. He has worked as a Casual Academic Teacher and an Exam Supervisor at Macquarie University, Sydney, Australia.

His research interests include antenna design and wave propagation, rain attenuation, and microwave and satellite communication. He received an International Macquarie Research Excellence Scholarship (iMQRES) from Macquarie University, in 2018, to pursue his Ph.D. degree, and a Professor Scholarship from Chosun University to accomplish a master's degree.



SYED MUZAHIR ABBAS (Senior Member, IEEE) received the B.Sc. degree in electrical (telecommunication) engineering from the COMSATS Institute of Information Technology (CIIT), Islamabad, Pakistan, in 2006, the M.Sc. degree in computer engineering from the Center for Advanced Studies in Engineering (CASE), Islamabad, in 2009, and the Ph.D. degree in electronics engineering from Macquarie University, North Ryde, NSW, Australia, in 2016. He has been

a Transmission Engineer at Alcatel-Lucent, Pakistan, a RF Engineer with CommScope, Australia, and a Senior Antenna Design Engineer with Benelec Technologies, Australia. He has lectured various courses at CIIT, Western Sydney University, Australia, Macquarie University, and The University of Sydney, Australia. He is currently working as a Senior Principal Engineer with Benelec Technologies. He has been a Visiting Researcher with the ElectroScience Laboratory, The Ohio State University, USA, and Queen Mary University of London, U.K. His research interests include base station antennas, mmWave antennas, high-impedance surfaces, frequency selective surfaces, flexible/embroidered antennas, CNT yarns, CNT/graphene-based antennas, reconfigurable antennas/electronics, and the development of antennas for UWB and WBAN applications. He has also received several prestigious awards and fellowships, including the 2012 iMQRES Award for Ph.D. degree, the Research Productivity Awards from CIIT, in 2012 and 2010, the 2013 CSIRO Postgraduate Fellowship, the 2018 Young Scientist Award (Commission B—Field and Waves) from the International Union of Radio Science (URSI), the 2019 IEEE NSW Outstanding Young Professional Award, and the 2020 IEEE 5G World Forum Best Paper Award.



MOHSEN ASADNIA (Senior Member, IEEE) received the Ph.D. degree in mechanical engineering from Nanyang Technological University (NTU), Singapore, in 2014. He undertook his postdoctoral training with the SMART Center, Massachusetts Institute of Technology, Cambridge, MA, USA, and The University of Western Australia (UWA), Perth, WA, Australia. He has been a Group Leader with Macquarie University, Sydney, NSW, Australia, since 2016,

where he is currently an Associate Professor and a Group Leader with the School of Engineering. His research interests include ion selective membranes, chemical sensors, MEMS/NEMS bio-inspired sensory systems, biomimetic devices, artificial hair cells of the vertebrate inner ear, and microfluidic devices.



KARU P. ESSELLE (Fellow, IEEE) received the B.Sc. degree (Hons.) in electronic and telecommunication engineering from the University of Moratuwa, Sri Lanka, and the M.A.Sc. and Ph.D. degrees in electrical engineering from the University of Ottawa, Canada.

Previously, he was the Director of the WiMed Research Centre and the Associate Dean—Higher Degree Research (HDR) with the Division of Information and Communication Sciences and directed the Centre for Collaboration in Electromagnetic and Antenna Engineering, Macquarie University, Sydney. He was a member of the Dean's Advisory Council and the Division Executive. He was the Head of the Department several times. He is currently the Distinguished Professor in electromagnetic and antenna engineering at the University of Technology Sydney and a Visiting Professor with Macquarie University. He is also the Director of Innovations for Humanity Pty Ltd. He has provided expert assistance to more than a dozen companies, including Intel, Hewlett Packard Laboratory, USA, Cisco Systems, USA, Audacy, USA, Cochlear, Optus, ResMed and Katherine-Werke, Germany. He led the team that designed the high-gain antenna system for the world's first entirely Ka-band CubeSat made by Audacy, USA, and launched to space by SpaceX, in December 2018. This is believed to be the first Australian-designed high-gain antenna system launched to space, since CSIRO-designed antennas in Australia's own FedSat launched, in 2002. His research has been supported by many national and international organizations, including Australian Research Council, Intel, U.S. Air Force, Cisco Systems, Hewlett-Packard, Australian Department of Defence, Australian Department of Industry, NSW Chief Scientist and Engineer Office, SmartSat Corporate Research Centre, and German and Indian governments. Since 2002, his research team has been involved with research grants, contracts, and Ph.D. scholarships worth over 25 million dollars, including 15 Australian Research Council grants. He has authored over 650 research publications and his papers have been cited over 13,000 times. In 2021, his publications received over 1,400 citations. His H-index is 53 and i-10 is 220. His research activities are posted in the web at (<http://web.science.mq.edu.au/~esselle/> and <https://www.uts.edu.au/staff/karu.esselle>).

Dr. Esselle is a fellow of the Royal Society of New South Wales and Engineers Australia. He was a recipient of 2004 Innovation Award for best invention disclosure, 2009 Vice Chancellor's Award for Excellence in Higher Degree Research Supervision, 2011 Outstanding Branch Counsellor Award from IEEE Headquarters (USA), 2012 and 2016 Engineering Excellence Awards for Best Published Paper from IESL NSW Chapter, 2017 Certificate of Recognition from IEEE Region 10, 2017 Highly Commended Research Excellence Award from Macquarie University, 2017 Engineering Excellence Award for Best Innovation, 2017 Excellence in Research Award from the Faculty of Science and Engineering, 2019 ARC Discovery International Award, 2019 Macquarie University Research Excellence Award for Innovative Technologies, 2019 Motohisa Kanda Award (from IEEE USA) for the most cited paper in IEEE TRANSACTIONS ON ELECTROMAGNETIC COMPATIBILITY in the past five years, 2020 IEEE NSW Outstanding Volunteer Award, Runner-up to the same prize, in 2020, 2021 IEEE Region 10 (Asia-Pacific) Outstanding Volunteer Award, and Finalist for 2021 Australian national Eureka Prize for Outstanding Mentor of Young Researchers. His other most recent awards include the top Space award in Australia—the “Winner of Winners” Excellence Award and the Academic of Year Award at the 2022 Australian Space Awards, Engineers Australia 2022 Sydney Professional Engineer of the Year and Bradfield Awards (in addition to the national title mentioned previously), both the most prestigious Excellence Award, and the Academic

of the Year Award at 2021 Australian Defence Industry Awards. He is an Australia's 2022 Professional Engineer of the Year. His mentees have been awarded many fellowships, awards, and prizes for their research achievements. 58 international experts who examined the theses of his Ph.D. graduates ranked them in the top 5% or 10%. Two of his students were awarded Ph.D. with the highest honor at Macquarie University—the Vice Chancellor's Commendation, and one received University Medal for Master of Research. In addition to the IEEE Kanda Award mentioned above, several of his papers have been among most cited or most downloaded. Often one or two of his papers are ranked by Web of Science and Clarivate as Highly Cited Papers (top 1% in the academic field of Engineering). For example, two papers are ranked so, for citations received, in January 2022 and February 2022. Some papers have been ranked as Hot Papers as well (top 0.1% in Engineering), e.g., A Scientific Reports paper for citations received, in January 2022 and February 2022. According to the Special Report on Research published by The Australian national newspaper, he is the 2019 National Research Field Leader in Australia in both micro-electronics and electromagnetism fields. He has served or is serving as a Senior Editor for IEEE ACCESS; an Associate Editor for IEEE TRANSACTIONS ON ANTENNAS PROPAGATION, *IEEE Antennas and Propagation Magazine*, and IEEE ACCESS; and the Lead Guest Editor of several journals, including IEEE ANTENNAS AND WIRELESS PROPAGATION LETTERS. From 2018 to 2020, he chaired the Prestigious Distinguished Lecturer Program Committee of the IEEE Antennas and Propagation (AP) Society, the premier global learned society dedicated for antennas and propagation, which has close to 10,000 members worldwide. After two stages in the selection process, he was also selected by this Society as one of two candidates in the ballot for 2019 President of the Society. Only three people from Asia or Pacific apparently have received this honor in the 68-year history of this Society. He is also one of the three distinguished lecturers (DL) selected by the Society, in 2016. He is the only Australian to chair the AP DL Program ever, the only Australian AP DL in almost two decades, and second Australian AP DL ever (after UTS Distinguished Visiting Professor Trevor Bird). He has served the IEEE AP Society Administrative Committee in several elected or ex-officio positions (2015–2020). He is also the Chair of the Board of Management of Australian Antenna Measurement Facility. He was the Elected Chair of IEEE New South Wales (NSW) and IEEE NSW AP/MTT Chapter, in 2016 and 2017, respectively. He is with the College of Expert Reviewers of the European Science Foundation (2019–2022) and he has been invited to serve as an International Expert/a Research Grant Assessor by several other research funding bodies as well, including the European Research Council and funding agencies in Norway, Belgium, The Netherlands, Canada, Finland, Hong Kong, Georgia, South Africa, and Chile. He has been invited by Vice-Chancellors of Australian and overseas universities to assess applications for promotion to professorial levels. He has also been invited to assess grant applications submitted to Australia's most prestigious schemes, such as Australian Federation Fellowships and Australian Laureate Fellowships. In addition to the large number of invited conference speeches he has given, he has been an invited plenary/an extended speaker/a keynote speaker/a distinguished speaker of several IEEE and other venues over 30 times, including EuCAP 2020 Copenhagen, Denmark; URSI'19, Seville, Spain; and 23rd ICECOM 2019, Dubrovnik, Croatia. He is the Track Chair of IEEE AP-S/URSI 2022 Denver, 2021 Singapore and 2020 Montreal; the Technical Program Committee Co-Chair of ISAP 2015, APMC 2011, and TENCON 2013, and the Publicity Chair of ICEAA/IEEE APWC 2016, IWAT 2014, and APMC 2000.

...